



Publication Year	2022
Acceptance in OA	2022-03-29T14:16:44Z
Title	Accretion and outflows in young stars with CUBES
Authors	ALCALA', JUAN MANUEL, CUPANI, Guido, Evans, C. J., FRANCHINI, Mariagrazia, NISINI, Brunella
Publisher's version (DOI)	10.1007/s10686-022-09832-1
Handle	http://hdl.handle.net/20.500.12386/32050
Journal	EXPERIMENTAL ASTRONOMY

Accretion and Outflows in Young Stars with CUBES

J.M. Alcalá · G. Cupani · C. J. Evans · M. Franchini · B. Nisini

Received: date / Accepted: date

Abstract The science case on studies of accretion and outflows in low-mass ($<1.5M_{\odot}$) young stellar objects (YSOs) with the new CUBES instrument is presented. We show the need for a high-sensitivity, near-ultraviolet (NUV) spectrograph like CUBES, with a resolving power at least four times that of X-Shooter **and combined with UVES** via a fibrelink for simultaneous observations. Simulations with the CUBES exposure time calculator and the end-to-end software show that a significant gain in signal-to-noise can be achieved compared to current instruments, for both the spectral continuum and emission lines, including for relatively embedded YSOs. Our simulations also show that the low-resolution mode of CUBES will be able to observe much fainter YSOs ($V \sim 22$ mag) in the NUV than we can today, allowing us extend studies to YSOs with background-limited magnitudes. The performance of CUBES in terms

of sensitivity in the NUV will provide important new insights into the evolution of circumstellar disks, by studying the accretion, jets/winds and photo-evaporation processes, down to the low-mass brown dwarf regime. CUBES will also open-up new science as it will be able to observe targets that are several magnitudes fainter than those reachable with current instruments, facilitating studies of YSOs at distances **of \sim kpc scale**. This means a step-change in the field of low-mass star formation, as it will be possible to expand the science case from relatively local star forming regions to a large swathe of distances within the Milky Way.

Keywords Stars: pre-main sequence, low-mass – Accretion, accretion disks – protoplanetary disks · stars: variables: T Tauri · CUBES instrument

Based on observations made with the VLT under programs 089.C-0143(A) and 097.C-0741(A)

J.M. Alcalá
INAF-Osservatorio Astronomico di Capodimonte, via
Moiariello 16, 80131 Napoli, Italy
E-mail: juan.alcala@inaf.it

G. Cupani
INAF-Osservatorio Astronomico di Trieste, Via G.B.
Tiepolo, 11, I-34143 Trieste, Italy
IFPU–Institute for Fundamental Physics of the Universe,
Via Beirut, 2, I-34151 Trieste, Italy

C. J. Evans
UK Astronomy Technology Centre, Royal Observatory,
Blackford Hill, Edinburgh EH9 3HJ, UK

M. Franchini
INAF-Osservatorio Astronomico di Trieste, Via G.B.
Tiepolo, 11, I-34143 Trieste, Italy

B. Nisini
INAF-Osservatorio Astronomico di Roma, Via di Frascati
33, 00078 Monte Porzio Catone, Italy

1 Introduction

The study of protoplanetary disks is a rapidly growing research field. Protoplanetary disks play a pivotal role in determining the initial conditions for planet formation, and many of their characteristics are only now being unveiled by new observational facilities at high angular and spectral resolution, over a wide range of wavelengths, from X-ray to radio.

The way in which circumstellar disks evolve and form protoplanets is strongly influenced by the processes of mass accretion onto the star, ejection of outflows and photo-evaporation in winds of the disk material ([45], [28]). A proper understanding of the impact of these phenomena requires comprehensive study of different physical processes throughout the first 10^7 yr of the star-disk evolution.

Observationally, the study of these processes is conducted via multi-wavelength investigations, in particu-

lar by studying classical T Tauri stars (CTTS), which are young (a few 10^6 yr), very low- to solar-mass stars that are actively accreting mass from planet-forming disks. In the current magnetospheric-accretion paradigm for CTTS, the strong stellar magnetic fields truncate the inner disk at a few stellar radii ([27], [49]). Gas flows from this location onto the star along the stellar magnetic field lines, forming an accretion shock at the stellar surface. The heated ($T \sim 10^4$ K) optically-thick, postshock gas and optically-thin, pre-shock gas emits in the Balmer and Paschen continua and in many spectral lines ([45]). At the same time, magnetically driven winds carry away the angular momentum of the accreting gas, thereby preventing the star from spinning up. Meanwhile, the accretion shocks produce strong UV and X-ray emission (e.g. [18]) that irradiates and photo-evaporates the disk.

Through spectroscopic surveys of young stellar objects (YSOs) in nearby ($d < 500$ pc) star-forming regions, the mutual relationships between accretion, jets and disk structure have been addressed (e.g. [2], [36] [31] [57] [64]), but further aspects remained unexplored, mainly because of the low sensitivity and **in some cases** spectral resolution so far available in the near-ultraviolet (NUV). For instance, YSOs in distant (\sim **kpc scale**) star-forming regions, where low metallicity effects **may** have an important impact on the accretion process, have been poorly studied.

Development of the new Cassegrain U-Band Efficient Spectrograph (CUBES) for the Very Large Telescope (VLT) [76] **may** enable important progress in the investigation of accretion and winds-outflows in solar-type young stars.

In this contribution we present the CUBES science case on accretion and wind-outflows in YSOs. Henceforth we use the terms CTTS or YSOs to refer to solar-type young stellar objects. In Sect. 2 relevant previous work and the need for a NUV instrument with high spectral resolution and sensitivity for studies of YSOs is highlighted. In Sect. 3 the expected performances of CUBES on typical solar-type YSOs are presented, taking into account the possibility of a fibrelink to the Ultraviolet and Visible Echelle Spectrograph (UVES) on the VLT. For background context, Sect. 4 introduces relevant ongoing YSO projects that will influence CUBES operations, and in Sect. 5 we summarise some of the key topics in the field that CUBES will address. Finally, a summary and conclusions are presented in Sect. 6.

2 Previous work and the need for sensitivity and spectral resolution

2.1 Measurements of accretion rates

The mass accretion rate, \dot{M}_{acc} , can be derived from the energy released per unit time in the accretion shock (accretion luminosity L_{acc} ; see [40], [44]) given the stellar properties, in particular stellar mass M_{\star} and radius R_{\star} . Observationally, this requires measurements of excess flux in the continuum and lines with respect to similar non-accreting template stars. Such measurements are best performed at ultraviolet (UV) wavelengths ($\lambda < 4000$ Å) with the Balmer continuum excess emission and the Balmer jump (see [46], [47], [1], [2], [57], and references therein).

On the other hand, accretion is a highly variable process ([15], [48], [22], [73]) which leads to a range of \dot{M}_{acc} values for a given object when measured at different epochs (see [23], [24], [16]). Variability in YSOs induces dispersion in \dot{M}_{acc} hence, in the observed $\dot{M}_{\text{acc}} - M_{\star}$ and $\dot{M}_{\text{acc}} - M_{\text{disk}}$ scaling relationships, but cannot explain the large scatter of more than 2 dex in $\log \dot{M}_{\text{acc}}$ at a given YSO mass. Such scaling relationships are predicted by the theory of viscous disk evolution ([55], [45], [70] and references therein) but the $\dot{M}_{\text{acc}} - M_{\text{disk}}$ relationship has been confirmed observationally only recently by spectroscopic surveys in strong synergy with ALMA surveys of disks in star-forming regions ([9], [56], [67], [62]).

2.1.1 The Balmer continuum

The continuum excess emission in YSOs is most easily detected as Balmer continuum emission (see [72], [40] and references therein). Such continuum excess emission has been used in the past to derive the accretion luminosity, L_{acc} , by fitting the YSO spectra with the sum of the photospheric spectrum of a non-accreting template and the emission of a slab of hydrogen (see [46], [69], [57], [1], [2] and references therein). The accretion luminosity is given by the luminosity emitted by the slab. Figure 1 shows an example of the procedure in the region of the Balmer jump, applied to the X-Shooter spectrum of the T Tauri star GQ Lup.

In the case of X-Shooter spectra, the wide wavelength range (3000-25000Å) allows the stellar and accretion parameters to be self-consistently derived by finding the best fit among a grid of slab models and using the continuum UV-excess emission, while constraining both the spectral type of the target and the interstellar extinction towards it. The best fit is found by minimizing a χ^2_{like} distribution (see Fig. 1 in [58]).

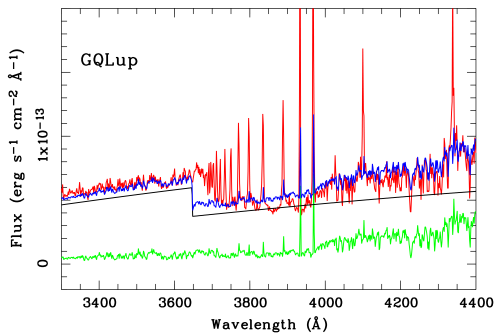


Fig. 1 Example X-Shooter spectrum of the classical T Tauri star GQ Lup in the region of the Balmer jump (in red). The spectrum of a non-accreting YSO template of the same spectral type as GQ Lup is shown in green. The continuum emission from a hydrogen slab is shown by the black continuous line. The best fit to the data with the emission predicted by the slab model is shown in blue. Figure adapted from [2].

The procedure requires a good absolute flux calibration (better than $\sim 15\%$) throughout the widest possible spectral range.

High sensitivity and spectral resolution in the NUV is needed for a better definition of the Balmer jump, and to improve the fit to the continuum. This is particularly important in cases of low accretion rates and YSOs with spectral types earlier than about K3, where the contrast is low between continuum excess emission and the photospheric + chromospheric emission ([3] and see Sect. 5.1.2). A sensitivity greater than e.g. X-Shooter is needed to detect the NUV excess emission in low-luminosity and slightly embedded YSOs.

2.1.2 $L_{\text{acc}}-L_{\text{line}}$ relationships: issues with high Balmer lines

It is well known that L_{acc} , and therefore \dot{M}_{acc} , is correlated with the line luminosity, L_{line} , of H I, He I and Ca II lines (e.g. [63], [19], [46], [69], [1], [2] and references therein). These latter works provide $L_{\text{acc}}-L_{\text{line}}$ correlations simultaneously and homogeneously derived from the UV to the near-infrared (NIR), underlying the importance of these emission features as accretion diagnostics. These accretion tracers are key diagnostics with which to estimate L_{acc} via the correlations mentioned above when flux-calibrated spectra below $\lambda \sim 3700 \text{ \AA}$ are not available. Examples of these correlations, drawn from measurements in X-Shooter spectra, are shown in Fig. 2.

At low L_{acc} values, detection of the high Balmer lines is challenging due to limited sensitivity. In fact, most of the lower-left points in Fig. 2 for the H15 line are represented by upper limits

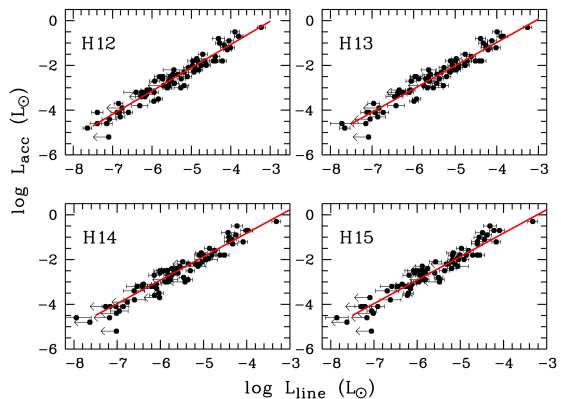


Fig. 2 Examples of $L_{\text{acc}}-L_{\text{line}}$ correlations for Balmer lines as labelled on each panel. Each point represents the L_{acc} and L_{line} measurement from the X-Shooter spectrum of an individual YSO. L_{acc} was determined from the slab modelling as explained in the text (see also Fig. 1), while L_{line} is calculated from flux measurements of the lines and adopting a distance to the individual YSO. Leftward arrows represent upper limits on L_{line} . The red lines represent the best linear fit to the data. Figure adapted from [2].

in L_{line} . As concluded in previous works (e.g. [69], [1], [4]), the average L_{acc} and \dot{M}_{acc} derived from several diagnostics, measured simultaneously, has a significantly reduced error and can also be used to simultaneously check the extinction. This argues for simultaneous spectroscopy from the UV to the longest practicable wavelengths, at the highest possible sensitivity.

Note that difficulties at the high Balmer lines may arise because of line blending, in particular when low resolution is used. Fig. 1 shows that the crowding of the high Balmer lines leads to blending that effectively shifts the Balmer limit from 3646 \AA to the apparent jump at $\sim 3700 \text{ \AA}$. Balmer lines in strongly accreting YSOs are intrinsically broad ($\Delta V \gtrsim 250 \text{ km/s}$) hence, the blending issues in such objects cannot be circumvented, even at the highest available resolution. A high resolution, however, may help studying the line profiles in more detail.

2.1.3 X-Shooter-UVES comparison

In this practical example we use data of the YSO Sz 88 A, a T Tauri star in the Lupus star-forming region. With an estimated $\dot{M}_{\text{acc}} \sim 3.2 \times 10^{-9} M_{\odot}/\text{yr}$ ([2], [3]), this star is an active accretor, hence its spectrum is rich in emission lines and exhibits strong continuum excess emission in the UV. The interstellar extinction toward the object is low ($A_V = 0.25 \text{ mag}$, [3]) and the source is suf-

ficiently bright ($V=13.2$ mag) for high-resolution spectroscopy with e.g. UVES.

A comparison of X-Shooter and UVES data¹ for this object, in the spectral region around the Balmer jump, is shown in Fig. 3. For comparison purposes, we have normalised the UVES data to the X-Shooter flux at 3660 Å.

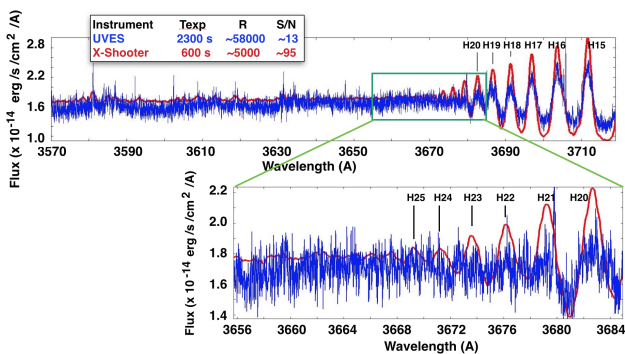


Fig. 3 Portions of the X-Shooter (red) and UVES (blue) spectra of the YSO Sz88A (large panel). The upper left insert shows the corresponding exposure times, resolutions and S/N ratios. A zoom of the region around the Balmer jump is shown in the lower panel. Balmer emission lines up to H 25 are labelled. The UVES data were normalised to the X-Shooter flux at 3660 Å.

Whereas UVES provides a spectral resolution that is more than a factor of ten larger than that from X-Shooter, the S/N ratio is seven times lower, despite the much longer exposure time, even in an object as bright as Sz 88 A. Lines up to H 25 can be detected in the X-Shooter spectrum, but they are not apparent in the UVES data because of the low S/N. For the same reason, structure is not seen in the line profiles in the UVES data. Note, however, that the X-Shooter spectrum was acquired more than four years before the UVES observation. Therefore, the non-detection of the high Balmer lines with UVES could be a consequence of lower accretion activity in Sz 88 A during the UVES observations. All this suggests the need for much higher sensitivity in the NUV than that of UVES when aiming at detection of emission diagnostics during low-accretion phases or in very weak accretors.

2.1.4 Physical conditions of the emitting gas

An important diagnostic for deriving the physical conditions (e.g. density and temperature) of the accreting gas is to use the H I line ratios, in particular by comparing the Balmer decrements with model predictions (e.g.

¹ Unpublished data from ESO programme 089.C-0143(A), PI. B. Nisini.

[51]). Based on the X-Shooter data by [2], [8] presented a detailed study of the Balmer, Paschen and Brackett decrements. These authors analysed the Balmer decrements up to the H 15 line, using H β (=H 4) as the reference value.

As shown in Fig. 3, lines up to H 25 were detected in the X-Shooter spectrum of Sz 88 A. Hence, we use these data here to exemplify the behaviour of the decrements in the high Balmer lines. Line fluxes were measured on the same X-Shooter spectrum, following the methodologies described in [2]. The fluxes were then corrected for interstellar extinction ($A_V=0.25$ mag, [2]) adopting the extinction curve from [33]. The resulting Balmer decrements are shown in Fig. 4. For the same reasons as discussed in [8] we also used the H β line as the reference value. At the X-Shooter resolution, the H ϵ (=H 7) line is not resolved from the Ca II λ 3969 Å line.

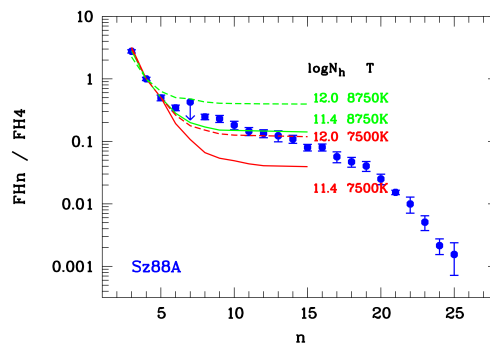


Fig. 4 Balmer decrements as a function of quantum number for the star Sz 88 A (blue dots), where the H β line ($n=4$) has been used as the reference value. The line ratio corresponding to H ϵ ($n=7$) is shown as an upper limit because of problems of blending with the Ca II λ 3969 Å line. The green and red continuous and dashed lines show models from [51] with densities and temperatures as labelled.

For lines up to about H 15 the Balmer decrements in Sz 88 A follow the type-4, or L-shape, trend as defined in [8]. As demonstrated by these authors, this L-shape decrement is very well described by models ([51]) of optically thick H I emitting gas with a temperature in the range 7500–8500 K and densities $11.4 < \log(N_H) < 12$ (see also the two lower-right panels in Fig. 11 of [8]). However, the trend of the decrements for lines with quantum number higher than ~ 15 inverts the slope, possibly indicating optically-thin emission from gas at lower temperature. This behaviour was also observed by [68] in the hydrogen spectrum of the brown dwarf 2MASS J05382543–0242412 (or σ -Ori 500) based on X-Shooter data. The authors concluded that the physical conditions of the emitting gas inferred from the hydrogen spectrum of this brown dwarf are in contrast with

the predictions of the magnetospheric accretion models, which predict much higher temperatures. This kind of analysis can only be performed for bright and highly accreting objects, **where the high-n Balmer lines can be detected**. However, the understanding of discrepancies with models requires accurate measurements of the Balmer decrement up to high n-number in samples of objects with different accretion activity, which requires **a greater sensitivity than so far available and the highest possible spectral resolution**.

2.2 Wind/outflow tracers

Mass loss through highly collimated jets and slow disk winds is a key mechanism driving accretion and contributing to disk dissipation. Previous X-Shooter surveys of YSOs ([64], [65]) have studied the rate of occurrence of collimated jets, deriving a tight link with the properties of slow winds, and establishing a relationship between the rate of mass loss in the outflow and the mass accretion rate ([65]).

While the [O I] 6300 Å line has provided the historical foundation for identifying and measuring jets and slow disk winds, for insights into the physical conditions of the different outflow manifestations one needs to observe several forbidden lines, probing different excitation regimes. **In this respect, a key line in the NUV spectral range is the [O II] line at 3726 Å as the [O II]3726/[O I]6300 flux ratio can be directly used to infer the plasma ionisation degree. The knowledge of the ionization degree is fundamental to infer the total gas density (once the electron density is known from other line ratios, such as the [O I]5577/6300 ratio) and thus to have a correct measurement of the mass-loss rate, which is a critical parameter to constrain the different models for disk dissipation and thus understand the protoplanetary disk evolution and planet formation (e.g. [50])**

Gas ionization is low in T Tauri outflows (e.g. 0.1-0.3) so this line is usually weak and therefore requires sensitive NUV observations to detect it in different sources. In addition, and as illustrated in Fig. 5, a spectral resolution higher than that provided by X-shooter is also needed to resolve the line into components at different velocities and thus measure the ionization fraction in each of them. This example effectively shows that the [O II] can be resolved into two components, possibly of low and high velocity, that cannot be resolved at the X-Shooter resolution. We note that the [O II] is a doublet at 3726.0/3728.8 Å and what we are seeing in Fig. 5 are two velocity components of the [O II]3726.0 Å line, separated by 0.7 Å i.e. about 56 km/s which is

a typical velocity separation in T Tauri outflows. The other component of the doublet at 3728.8 Å (at 2.8 Å from the 3726.0 Å line) is barely visible above the noise in the UVES spectrum, as expected having a radiative rate a factor of 10 smaller than the 3726.0 Å line.

Notably, the intensity of the forbidden line in Fig. 5 remains approximately the same, whereas the intensity of permitted lines, such as H 13 and H 14, is clearly changing. As mentioned before, the latter may be a consequence of variable accretion, as the UVES spectrum was acquired more than four years after the X-Shooter observation.

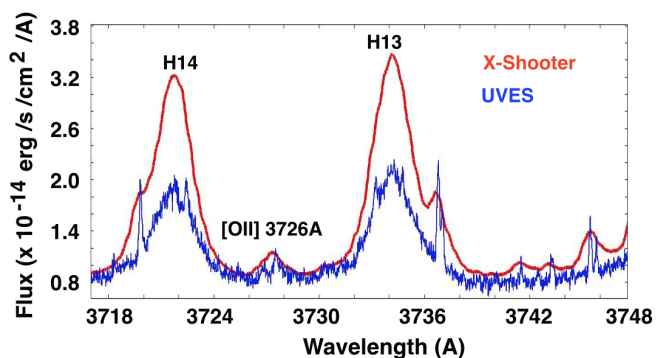


Fig. 5 Portions of the X-Shooter (red) and UVES (blue) spectra of Sz 88 A in a spectral range around the [O II] 3726 Å line. The spectra are the same as in Fig. 3. The UVES data were normalised to the X-Shooter flux at 3660 Å.

3 CUBES performance for YSO studies

The current topics in YSO studies and limits of observations outlined in Sect. 2 argue for a high-sensitivity spectrograph such as CUBES, with a resolving power at least four times that of X-Shooter, and possibly linked to UVES for simultaneous observations with both instruments. We now present results from simulations to quantify the potential performance of CUBES in the context of YSO studies.

The primary operational mode of CUBES is expected to have a resolving power $R \geq 20,000$ over the spectral range from 3000 Å to 4050 Å. Taking advantage of the high-sensitivity provided by CUBES in the near-UV, a second operational mode with $R \approx 7,000$ over the same spectral range is foreseen to allow the investigation of background-limited objects for science cases not requiring the high-resolution mode. In addition, a fibre-link to UVES for simultaneous observations at longer wavelengths is included in the conceptual design [76].

To investigate the instrument performance for the YSO cases we used the exposure time calculator (ETC)² and the end-to-end simulator (E2E) software³ developed for CUBES [35]. To apply these tools to our science case, accurately flux-calibrated spectral templates of YSOs are needed, with good S/N (>90) in the NUV, and with a resolution similar or higher than that expected for CUBES. Real spectra, simultaneously satisfying such characteristics, are not available, while reliable models of spectra reproducing the complete YSOs phenomenology do not yet exist. Real data that most closely satisfy these requirements are the X-Shooter spectra. Despite their lower resolution, the general spectral shape can be used to predict the S/N of the continuum (and the higher S/N expected for the emission lines). We therefore used these as our input templates, in particular those of the YSOs discussed in Sect. 2, namely GQ Lup and Sz 88 A. A shortcoming of the X-Shooter data is that the S/N drops significantly for $\lambda < 3250 \text{ \AA}$ hence, for simplicity, we set the flux to zero below this wavelength.

3.1 High-resolution mode

Bright objects ($V < 19 \text{ mag}$): We used the X-Shooter observation of GQ Lup (Sz 75; SpT=K6, [3]) as our input template, assuming $A_V=0 \text{ mag}$. We used the CUBES ETC to estimate the performance for $V=10 \text{ mag}$ and 19 mag , in adopted conditions of seeing=1 arcsec and airmass=1.2, with predicted S/N ratios (at $\lambda=3600 \text{ \AA}$) of ~ 320 and 10 , in 5 min and 1 hr, respectively. For an input template with a weak continuum Balmer emission, and with an earlier spectral type than GQ Lup (e.g. MY Lup, SpT=K0, [3]), slightly lower values of S/N are predicted, with S/N = 300 in 5 min and 9 in 1 hr for $V=10 \text{ mag}$ and 19 mag , respectively. Adopting $V=18.5 \text{ mag}$ (for the MY Lup template) we find S/N=14 in 1 hr; this magnitude is typical of YSOs in the low-metallicity region Sh2-284 [25].

Adopting a later M6 template (2MASS J16095628–3859518 or Lup818s in [1]) with $V=19 \text{ mag}$ and the same conditions in the ETC yielded S/N ≈ 10 in 1 hr. This example highlights the interesting prospect of systematically studying accreting brown dwarfs at relatively high resolution in the UV for the first time.

Faint objects ($V > 19 \text{ mag}$): For objects as faint as $V=20 \text{ mag}$, we use the X-Shooter data of Sz 88 A as the input template, which also has a very good S/N and was

used to exemplify the behaviour of the Balmer decrement in Sect. 2.1.4. This template is shown in the left-hand panels of Fig. 6 for the cases of $A_V=0$ and 3 mag of visual extinction. Using the CUBES ETC and adopting conditions of seeing=0.8 arcsec and airmass=1.2, we estimate a S/N of 12 and 6 at $\lambda=3600 \text{ \AA}$ for the two A_V values, respectively, in 1.5 hrs of exposure and with binning $\times 2$ in the spatial direction. The S/N ratio at 3600 \AA as a function of exposure time is shown in the right-hand panels of Fig. 6 for the two A_V values. We also used the E2E simulator with the same template and observing assumptions and recovered an estimated S/N that was in very good agreement with the ETC.

For comparison with the above results, we obtained S/N ≈ 5 at $\sim 3600 \text{ \AA}$ in our X-Shooter spectrum of the young brown dwarf 2MASS J05382543–0242412 (σ -Ori 500 with $V=20 \text{ mag}$, $A_V=0 \text{ mag}$, [68]). This 1.5 hrs exposure was done under similar conditions as those assumed for the ETC predictions above, meaning that in the faint example (with $A_V=0$) CUBES would provide data with twice the S/N and about four times better resolution than X-Shooter. In addition, the quality of the CUBES data for moderately embedded objects will be sufficient for the studies discussed in Sec. 5.

It is worth mentioning that the S/N ratio per pixel provided by the ETC does not take into account any optimal extraction of the 1-dimensional spectra and therefore the predicted S/N value is expected to improve in case of optimal extraction from the 2-dimensional images. Also, the S/N of the emission lines will be higher than for the continuum.

3.2 Low-resolution mode

We make use of the E2E software to simulate the low-resolution mode of CUBES, adopting the first configuration described in Sect. 4.2 of [35], which uses six slices of 1 arcsec each. With the same input parameters as in the previous subsection (Sz 88 A template, $V=20 \text{ mag}$, seeing = 0.8 arcsec, airmass=1.2, $T_{\text{exp}} = 1.5 \text{ hr}$, $\lambda = 3600 \text{ \AA}$) we obtained the results shown in Fig. 7, namely S/N values of 20 and 10 for the $A_V=0$ and 3 mag models, respectively, with a spatial binning $\times 4$ and wavelength binning $\times 3$ (which still yields a sampling well above the Nyquist limit). The noise breakdown histograms are also shown in the right-hand panels of the figure. Note the limited contribution of the target on the spectrograph arm ‘0’, which is due to the zero flux at $\lambda < 3250 \text{ \AA}$ in the input template.

This simple exercise shows that a significant gain in S/N, both in continuum and lines, can be achieved in the CUBES low-res. mode, and suggests that observations of even fainter YSOs can be attempted if

² <http://archives.ia2.inaf.it/cubes/#/etc>

³ <https://cubes.inaf.it/end-to-end-simulator>

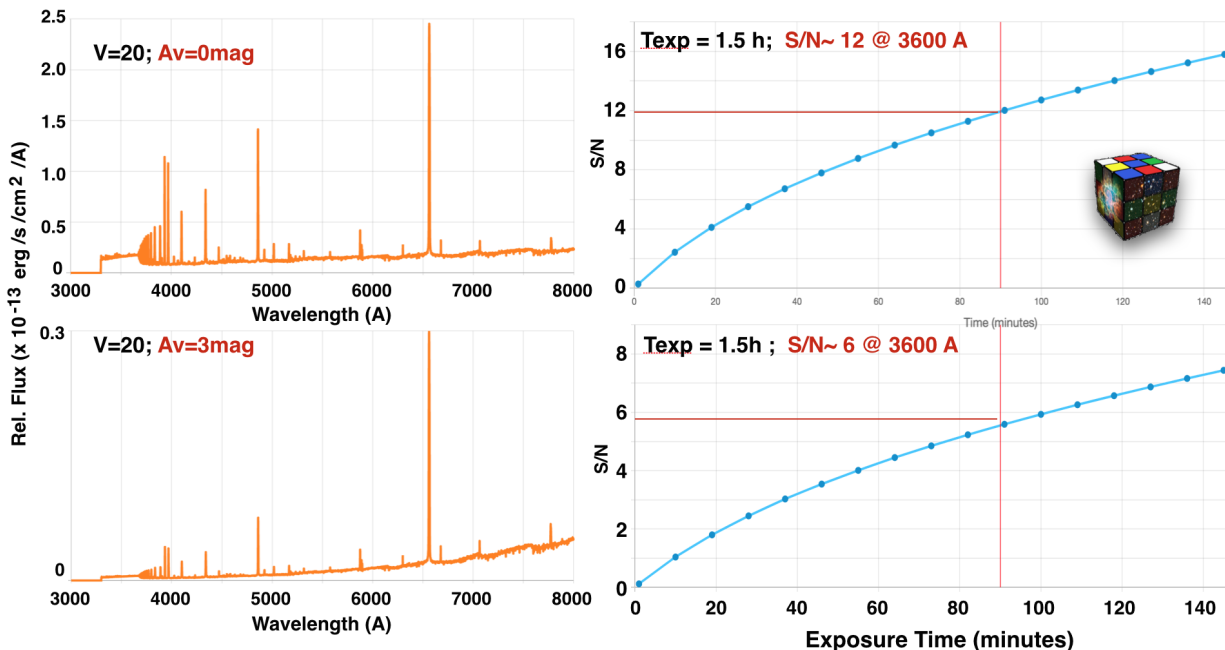


Fig. 6 Results of the CUBES ETC for the faint case discussed in the text. The template spectra for visual extinctions of $A_V=0$ and 3 mag are shown in the upper and lower left-hand panels, respectively. Note that the unreddened flux of the template corresponds to the actual magnitude of Sz 88 A ($V=13.2$ mag), but it is internally normalised to $V=20$ mag in the ETC. The ETC results, for the two A_V cases, are shown in the upper and lower right-hand panels, respectively for the exposure time as labelled. The blue curves with dots in the right-hand panels show the S/N ratio as a function of exposure time for $\lambda=3600$ Å. The resulting S/N ratios at 3600 Å are labelled in red. All the plots were extracted from the ETC.

we are able to trade spectral resolution for sensitivity. Hence, pushing to lower flux limits, for $V=22$ mag and $A_V=0$ mag, with $T_{\text{exp}}=2$ hr and adopting the same parameters as before, the E2E simulator yields the results shown in Fig. 8. The predicted S/N is ~ 5 at $\lambda=3600$ Å, but it is >10 for many emission lines, which opens-up the possibility to extend studies done with X-Shooter, but in YSOs with background-limited magnitudes.

We note that the result from the E2E simulator is the combination of the extracted spectra from all the instrument slices (see [35]); in our simulations we only use three slices but most of the object’s flux will go through the central slice, hence we expect an optimal extraction of this slice would further improve the final S/N, compared to the estimates shown here.

3.3 Link with UVES

The simultaneous fit of the Balmer continuum and physical parameters of YSOs is best when the widest possible spectral window is available, which requires observations that extend redwards far beyond the CUBES range (see Sect. 2). A fibrelink to UVES for observations with both instruments simultaneously would make this

possible. As accretion is a highly variable process, the simultaneous link is necessary for the fitting procedure described in Sect. 2.

Introducing a fibrelink entails a reduction in the UVES throughput, so this is only an efficient option if the performance of UVES with the fibrelink is sufficiently good to deliver the required observations within the time needed for CUBES observations. The conceptual design provides a 40% throughput for the fibre-link at >5000 Å. We estimated the exposure times required to reach a S/N=10, adopting the unreddened spectral template shown in Fig. 6 (in the reddened case, the NUV performance will be the more limiting factor); for airmass=1.2 and seeing=0.8 arcsec for:

- CUBES ETC: continuum near the [O II] 3726 Å line, $V=19.5$ mag, with the high-resolution option and binning $\times 2$ spatially, gives $S/N \approx 10$ in 1 hr.
- UVES ETC: continuum near the [O I] 6300 Å line, $V=20.5$ mag (scaled to mimic the reduced throughput of the fibrelink compared to normal UVES operations), with a 1.0” slit, and the red-arm (580 nm) setting. The latter combination gives a resolution $R \approx 40,000$ with sampling of >5 pixels. With 2×2 binning we recover a $S/N \approx 5.5$ in 1 hr. Binning this

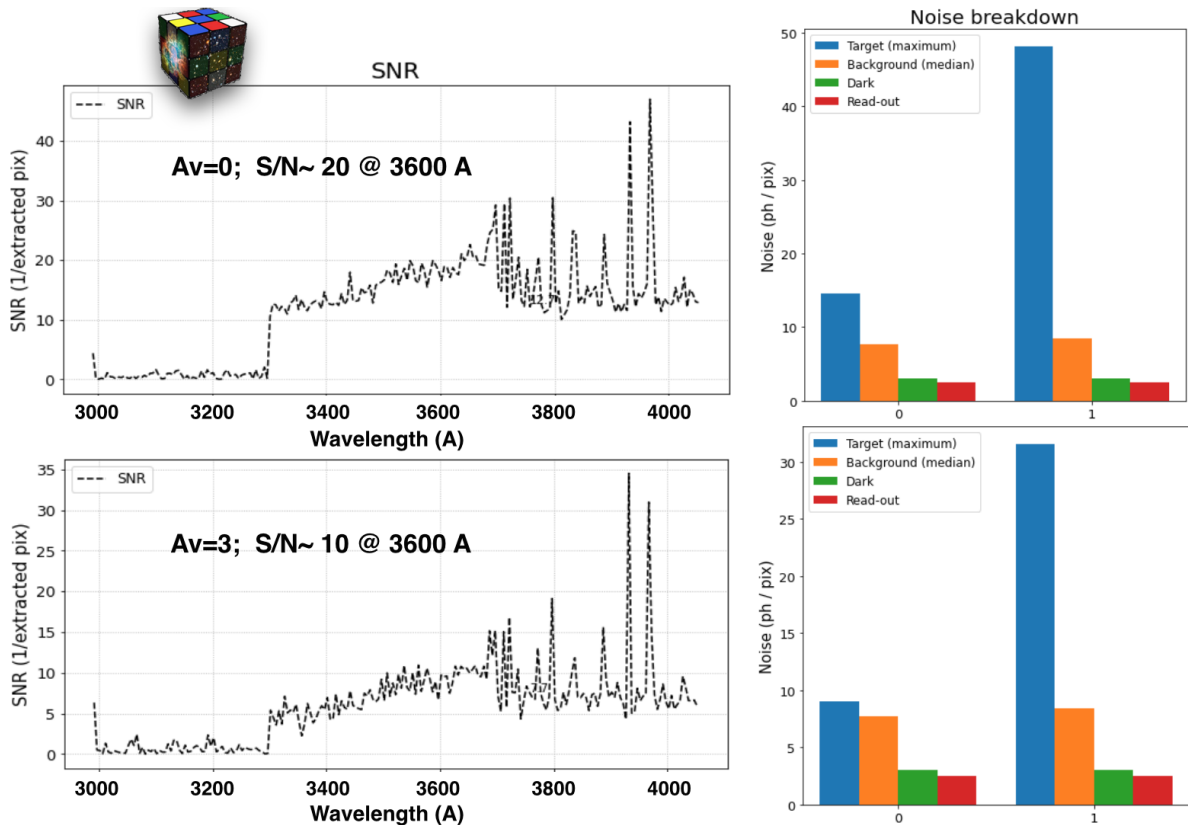


Fig. 7 Results from the CUBES E2E simulator for the low-resolution mode and the faint case ($V=20$ mag) discussed in the text. The left-hand panels show the resulting S/N as a function of wavelength for visual extinctions $A_V=0$ and 3 mag as indicated. Note the higher S/N of the emission lines with respect to the continuum and the zero S/N for $\lambda < 3250$ Å due to the cut of flux in the input X-Shooter data. The right-hand panels show the noise breakdown for the two corresponding A_V values. The two histograms in each panel are the photons/pixel of each component as coloured and labelled in the legend, for the two instrument arms (0 or 1 on the x-axis, the ‘blue’ and ‘red’ arms, respectively). Plots extracted from the E2E simulator.

by a further factor of three (oversampling, degrading resolution to match CUBES), gives a comparable S/N in a similar exposure time; i.e. the UVES exposure time fits within the CUBES observation.

Without the fibre link, a red-arm UVES exposure of ~ 1200 s gives comparable S/N (ignoring the preset and separate acquisition time), i.e. each combined (CUBES + UVES) observation effectively saves half an hour of otherwise separate UVES observations in this example.

4 Synergies with other projects

For background context of future programmes in this field, we now briefly introduce some on-going large programmes on YSOs that will have strong synergies with CUBES observations.

4.1 ALMA disk surveys

The Atacama Large Millimeter Array (ALMA) provides sufficient sensitivity and resolution at sub-mm wavelengths to detect and measure the mass, M_{disk} , of dusty protoplanetary disks around YSOs with a mass down to $0.1 M_{\odot}$ ([9], [10], [67], [14], [20]). Such surveys have provided the demographics of disks in nearby star-forming regions. The synergy of these surveys with the studies of the properties of the central objects, such as stellar mass, M_{\star} , and accretion rate, \dot{M}_{acc} , have provided important constraints on models of viscously evolving disks by confirming the correlations of M_{disk} with M_{\star} and \dot{M}_{acc} (see Sect. 5.1.3), although with significant scatter. However, these synergies did not include statistically significant samples of YSOs with $M_{\star} \leq 0.1 M_{\odot}$, preventing investigation of whether the scaling relationships are different for low-mass substellar objects to those for stars. Future sensitive ALMA surveys of compact and small disks in very low-mass YSOs, will

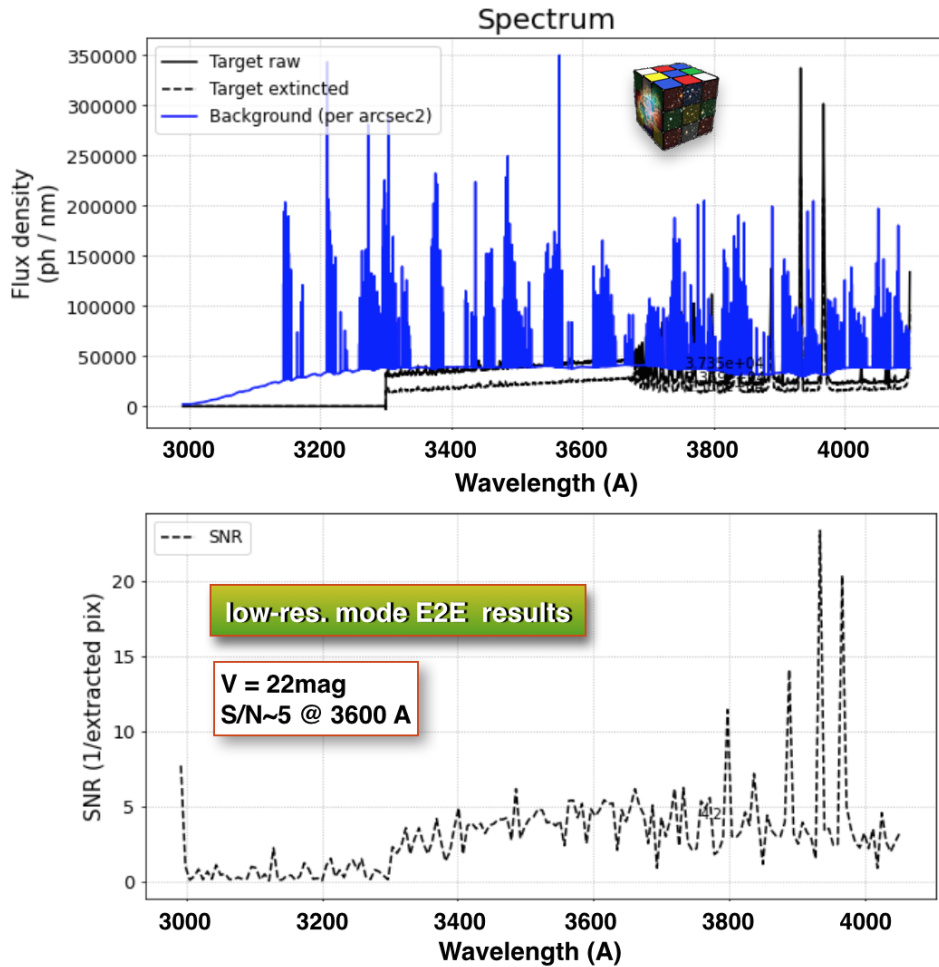


Fig. 8 Upper panel: the E2E input spectrum of Sz 88 A without (black continuous line) and with airmass (black dashed line) for the case of a $V=22$ mag YSO and $A_V=0$ mag.; the background contribution is shown with the blue line. Lower panel: the E2E output S/N as a function of wavelength (dashed line) for a 2 hour exposure. Note the zero S/N for $\lambda < 3250$ Å due to the cut of flux of the input X-Shooter data. Plots extracted from the E2E simulator.

allow investigation of the correlations down to the low-mass brown dwarf regime.

4.2 ULLYSES & ODYSSEUS

The public *Hubble Space Telescope* UV Legacy Library of Young Stars as Essential Standards (ULLYSES) survey will enable significant advances in the study of astrophysical disk accretion processes. A total of 500 orbits of this Directors Discretionary Time programme has been dedicated to far-UV spectroscopy with the Cosmic Origins Spectrograph (at $R \approx 18,000$) and low-resolution NUV/optical spectroscopy with the Space Telescope Imaging Spectrograph of tens of solar-type YSOs. The targets cover a range in stellar mass, accretion rate, and age (e.g., [2], [57]).

A large, international team has initiated the Outflows and disks around Young Stars: Synergies for the Exploration of ULLYSES Spectra (ODYSSEUS) project to bring together the broad expertise required to resolve the fundamental problems on accretion and wind on YSOs through the investigations enabled by ULLYSES [29], and to coordinate the ambitious datasets of simultaneous and contemporaneous observations that will enhance the impact of the public data (e.g. PENELLOPE [59]). We anticipate strong synergies of future CUBES observations of YSOs with ODYSSEUS science products.

4.3 PENELLOPE

The ESO large program (106.20Z8) PENELLOPE ([59], [32]) at the VLT is providing contemporaneous high-

resolution (UVES, ESPRESSO) and UV-NIR mid-resolution (X-Shooter) spectra of the ULLYSES targets to provide their accretion/ wind and stellar physical and kinematical properties. The project involves more than 50 researchers and, together with ODYSSEUS, will provide well characterized targets in terms of accretion/wind and stellar properties. These will then serve as a bright benchmark sample for CUBES programmes.

4.4 GHOS T

The GIARPS High-resolution Observations of T Tauri stars (GHOS T) ([38], [34], [4]) is a GIARPS@TNG optical/IR high-resolution spectroscopic survey of a flux-limited, complete sample of T Tauri stars in the Taurus star-forming region. This ongoing survey will homogeneously derive (i.e. avoiding systematics due to non-simultaneous observations) stellar and accretion/outflow parameters of sources in Taurus, and constrain the properties of the gas in the inner disk regions. This survey is in synergy with existing ALMA disk observations in the region (e.g. [54]), so the programme will directly link the processes occurring in the star-disk interaction region and the overall disk structure, providing a unique, rich, and robust observational reference for disk evolutionary models.

5 Studies of YSOs with CUBES

The high performance of CUBES in terms of spectral resolving power and sensitivity will **mostly** broaden our knowledge on accretion and outflows in YSOs, but will also open-up new science as it will be able to observe targets that cannot be reached with current facilities. In this section we describe some of the YSO topics that can be addressed with CUBES, and with the proposed link to UVES. **Except for line profile analysis (line shapes and peak position, widths and kinematics), these studies require a good absolute flux calibration ($\sim 15\%$ or better, see Sect. 2.1) throughout the widest spectral range. Shouldn't this requirement be satisfied by the simultaneous CUBES + UVES combination, a contemporaneous photometric follow-up, from the NUV to the reddest possible wavelength, will be necessary.**

5.1 Accretion

High throughput observations at $R \geq 20,000$ will enable more detailed study of the accretion process than currently possible, via precise modelling of the Balmer

jump, and **by studying the higher-order Balmer lines.** The high Balmer and Ca II H (3968 Å) & K (3933 Å) lines provide diagnostics of the accretion funnel flows and heated chromosphere in the post-accretion shock region (e.g., [5]).

As shown in Sect. 3.2, observations of objects down to $V=22$ mag with CUBES will be possible with the low-res. mode. By scaling the X-Shooter spectrum of Sz 88 A ($V=13.2$ mag) to $V=22$ mag, we derived line fluxes a factor $\sim 3 \times 10^{-4}$ lower than those discussed in Sec 2.1.4. **Thus, considering the Gaia DR2 distance of 158 pc for Sz 88 A and assuming $A_V=0$ mag it would be in principle possible to observe strong accretors similar to Sz 88 A up to a distance of ~ 9 kpc with CUBES,** with line fluxes in the range from 7.5×10^{-16} to 2.2×10^{-17} erg s $^{-1}$ cm 2 , respectively for the Balmer lines from H α to H 15, and down to 4.2×10^{-19} erg s $^{-1}$ cm 2 for H 25. **However, the average empirical rule of one magnitude of extinction per kpc, implies $A_V \approx 9$ mag. at 9 kpc. In addition, extinction may be much higher towards the galactic plane.**

As seen in the previous subsections the high-res. mode offers the possibility of observations of relatively reddened ($A_V=3$ mag) YSOs with $V=20$ mag (see Sect. 3.1), which translates to objects similar to Sz 88 A at a distance of up to ~ 3.5 kpc.

In the case of very low-mass objects ($M_* < 0.1 M_\odot$), such as 2MASS J16095628–3859518 (or Lup 818s in [1] and [3]; SpT=M6; $V \approx 18$ mag; $\log L_{\text{acc}} = -4.31$; $\log \dot{M}_{\text{acc}} = -10.96$) in Lupus, the limiting $V=22$ mag in the low-res. mode implies a dilution in flux by a factor $\sim 2.5 \times 10^{-2}$, theoretically meaning a **limiting $\log(L_{\text{acc}}) \approx -6$ and $\log(\dot{M}_{\text{acc}}) \lesssim -11$, with L_{acc} and \dot{M}_{acc} in units of L_\odot and $M_\odot \text{ yr}^{-1}$, respectively.**

5.1.1 High Balmer lines and physical conditions of accreting gas

Our previous studies with X-Shooter ([1], [2], [8]) showed an important similarity of the physical conditions in the accreting gas for objects with very different \dot{M}_{acc} , which was suggested by a number of properties. One was the comparable behaviour of the Balmer decrements down to H 15 for different objects, while another was the similarity of the $L_{\text{acc}}-L_{\text{line}}$ relations which, to zeroth order, are linear, with slopes varying between 0.99 and 1.18 for the hydrogen lines, and 0.90 to 1.16 for the He I lines. This means that, over a range of five orders of magnitude in L_{acc} , a similar fraction of the accretion energy is emitted in each line, independently of their excitation potential and optical depth. This is shown in Fig. 9 where the fractional line luminosities ($L_{\text{line}}/L_{\text{acc}}$) for a

few example lines are plotted as a function of L_{acc} in log scale. We used the $L_{\text{acc}}-L_{\text{line}}$ relationships by [1] to produce this plot. The relations are very stable across the examined stellar parameters, suggesting that the physical conditions of the accreting gas are very similar in all objects. Some evidence of a different behaviour of the Balmer decrements at high Balmer lines, possibly indicating different physical conditions of the accreting gas, were discussed in Sect. 2.1.4.

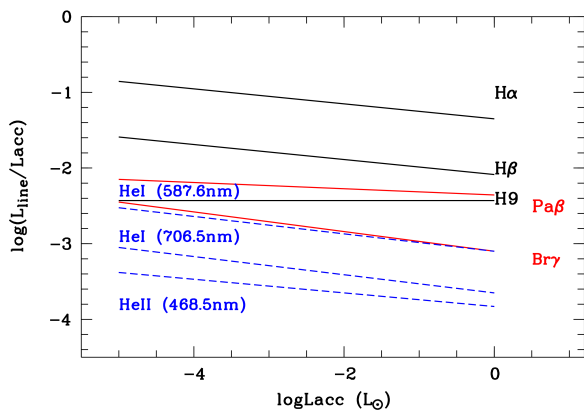


Fig. 9 Fractional $L_{\text{line}}/L_{\text{acc}}$ line luminosity as a function of L_{acc} in log scale for example diagnostic lines as labelled. The relationships between line luminosity and accretion luminosity by [1] were used to produce the plot.

CUBES observations of relatively bright YSOs (with $V < 19$ mag) in the high-res. mode will allow us to investigate the decrements in a more detailed fashion, as well as extending the $L_{\text{acc}}-L_{\text{line}}$ calibrations to the high-order Balmer lines hence, further investigate the physical conditions of the accreting gas at high quantum numbers. The ODYSSEUS-PENELLOPE and GHOT projects (see Sect. 4) will provide bright and very well characterised targets (in terms of physical and accretion properties) that will be perfect targets for CUBES observations. The extended $L_{\text{acc}}-L_{\text{line}}$ calibrations will be critical for estimates of L_{acc} in much fainter objects, where fits to the Balmer jump will not be possible because of the low S/N of the continuum, but where the emission lines are expected to be well detected.

CUBES would be in principle self-sufficient for this studies, while the simultaneous UVES link would provide more diagnostics in the red for a more complete analysis. The resolution of CUBES will also be **helpful** for the analysis of the line profiles, providing further information on the physical and kinematical properties of the accreting gas (e.g. [8]).

5.1.2 Accretion at advanced stages

Transition disks (TDs) are protoplanetary disks that show evidence of inner holes and gaps, as observed in millimeter interferometric observations ([6], [71], [7]) and in the dip of the mid-IR spectral energy distribution (e.g. [60]). The leading explanation for the presence of inner holes and gaps in the dust distribution of TDs is photo-evaporation (e.g. [28], [71]).

Low-mass pre-main-sequence stars with transitional disks accreting at very low rates are likely in the final stages of inner disk evolution, and probably have already formed proto-planets ([66]). Hence, identifying and investigating such slow accretors may help us to understand planet formation. However, measurements of low \dot{M}_{acc} are challenging. In general, weak accretion is not easily detectable in the region of the Balmer jump. Some previous studies attempted \dot{M}_{acc} measurements in TDs using other tracers, such as trends between the lines width and \dot{M}_{acc} (e.g. [61], [21]). However, such estimates depend heavily on rather uncertain scaling relations (see discussion in [1]). Using the $L_{\text{acc}}-L_{\text{line}}$ relationships is in principle possible. However, at very low accretion levels the chromospheric contribution to the emission budget may be comparable to L_{acc} and must therefore be disentangled.

Another important aspect regarding YSOs in advanced stages is represented by possible degeneracy of stellar and accretion parameters in objects with spectral types earlier than about K3. In these relatively early-type objects the low contrast between the continuum excess emission and the photospheric + chromospheric emission, may prevent a reliable assessment of accretion. For example, Fig. 10 shows the case of the star MY Lup; the solution on the accretion parameters based on low-res. spectra alone may be ambiguous, with up to an order of magnitude difference in L_{acc} (see e.g. [3]). CUBES will allow us to measure low accretion rates, by more precisely disentangling the contribution from chromospheric emission, which is difficult to remove **in general, but practically impossible if S/N is low in the NUV. The simultaneous link with UVES will improve the fitting of continuum excess emission.**

5.1.3 Low end of \dot{M}_{acc} in large surveys

A crucial prediction of the YSO viscous accretion theory is the existence of correlations between the disk mass (M_{disk}) the stellar mass (M_{\star}) and the mass accretion rate (\dot{M}_{acc}) ([45]). Such correlations have been confirmed only recently for the disk populations of the 1-3 Myr old Lupus and Chamaeleon I star-forming re-

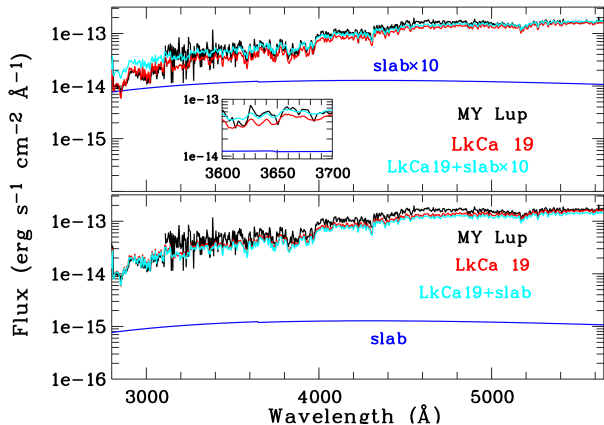


Fig. 10 Lower panel: extinction corrected low-resolution spectra of MY Lup (in black) and the non-accreting template LkCa 19 (in red). The slab model derived in [2] is also shown (in blue). The cyan spectrum shows the sum of the non-accreting template plus the slab emission. Upper panel: as per the lower panel, but now with the slab model multiplied by ten. Note the tiny Balmer jump shown in the inset. Figure adapted from [3].

gions (see Sect. 4.1 and [56] and references therein). The observed relations show, however, a much larger scatter in \dot{M}_{acc} (>0.9 dex) than viscous evolution would predict for 1-3 Myr old populations. The viscous disk theory predicts a smaller spread of \dot{M}_{acc} (<0.4 dex) at older ages. We thus need to measure the spread of \dot{M}_{acc} at given M_{disk} for carefully selected samples of relatively old YSOs, where accretion activity is expected to be weak. Recent work with X-Shooter showed the existence of very high accretion rates in the (>5 Myr) Upper Scorpius association. CUBES will contribute by measuring the weak Balmer jump and weak excess emission, as well as disentangling the contribution of the chromospheric emission.

Another important point which deserves further investigation is that there is growing evidence of a change in the slope of the $M_{\star}-\dot{M}_{\text{acc}}$ relationship for CTTS with ages of 2-3 Myr at $M_{\star} < 0.2 M_{\odot}$ ([57] and [2], and see Fig. 11). Such a break could be related to a faster disk evolution at low-masses (e.g. [74]). To verify this, the slope of the $\dot{M}_{\text{acc}}-M_{\star}$ relationship needs to be sampled at much lower M_{\star} and \dot{M}_{acc} values than done so far. In Fig. 11 the **theoretical** limits that CUBES may be able to reach are shown with the instrument logo. Note that such limits are much lower than the values for σ -Ori 500 (2MASS J05382543–0242412), the V= 20 mag young brown dwarf discussed in Sect. 2.1.4.

CUBES not only will complement the surveys of 1-2 Myr clusters with accurate \dot{M}_{acc} determinations, but its sensitivity will allow us to investigate the accretion process in young brown dwarfs, possibly down to

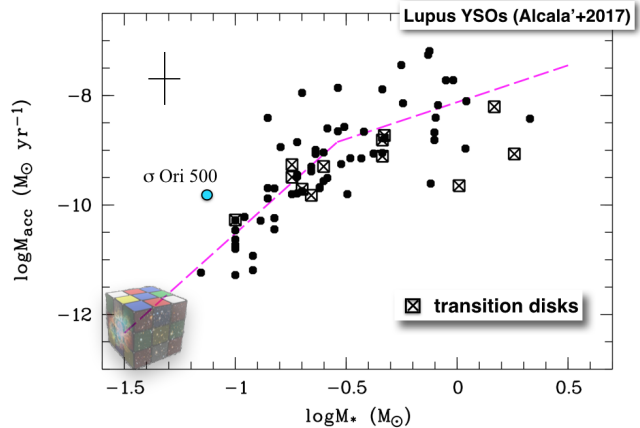


Fig. 11 Mass accretion rate (\dot{M}_{acc}) as a function of stellar mass (M_{\star}) for YSOs in the Lupus clouds (black symbols). Transitional disks are shown with crossed squares. The position of the young brown dwarf 2MASS J05382543–0242412 (or σ -Ori 500) is shown with the blue dot. Average errors in $\log(\dot{M}_{\text{acc}})$ and $\log(M_{\star})$ are shown in the upper left. Dashed magenta lines represent the fits to the data as in Eqs. (4) and (5) from [2]. The CUBES logo shows the region of the diagram that the instrument may be able to reach. Figure adapted from [3].

$M_{\star} \sim 30 M_{\text{Jup}}$ and $\dot{M}_{\text{acc}} \lesssim 10^{-11} M_{\odot}/\text{yr}$. By studying the $\dot{M}_{\text{acc}}-M_{\star}$ relationship at such limits it will be possible to investigate whether low-mass objects have indeed a faster disk evolution than their more massive counterparts, as proposed by some disk accretion models ([74]).

Finally, another important issue regards the validity of the $L_{\text{acc}}-L_{\text{line}}$ relationships at the very low-mass regime. Recently [11] have produced a theoretical $L_{\text{acc}}-L(\text{H}\alpha)$ relationship drawn from modelling of a shock at the surface of a planetary mass object. These authors show that the new theoretical relationship yields a much higher L_{acc} for a given $L(\text{H}\alpha)$ than what the relationships drawn from YSO spectra would predict. Hence, the validation of the relationships at the lowest possible mass is of key importance.

The high-sensitivity makes of CUBES a self-sufficient instrument for the studies of accretion in very-low mass YSOs, although the simultaneous link with UVES would be helpful for the YSO classification.

5.1.4 \dot{M}_{acc} in low metallicity environments

A very important aspect that has received little attention so far, mainly because of the limited sensitivity of the existing intermediate/high resolution instruments, is the spectroscopic study of YSOs in distant (**a few**

kpc) star-forming regions. At such distances, the low metallicity may have an important impact on accretion.

Photometric studies in low-metallicity regions (e.g. [26], [17] and references therein) suggest that metal-poor stars accrete at higher rates than solar-metallicity stars in nearby Galactic star-forming regions. As a consequence, most stars forming in a low-metallicity environment should experience disk dispersal at an earlier stage (in less than about 1 Myr) than those forming in solar metallicity environments (where disk dispersal may last up to 5-6 Myr). Thus, metallicity may play a crucial role on circumstellar disk evolution, hence on the time scale available for planet formation.

Typical solar-mass YSOs at kpc distances are faint ($V > 18$ mag, see [25]) so require the significant increase in sensitivity that CUBES will provide compared to current instruments. CUBES observations will allow us to investigate the Balmer jump, hence L_{acc} and \dot{M}_{acc} at low Z ($< 0.2 Z_{\odot}$) and answer questions such as: are the $L_{\text{acc}}-L_{\star}$ relationships the same at Solar metallicity? Are the Balmer decrements similar to those at Solar metallicity? What are the effects of local and external UV radiation fields (i.e. external photo-evaporation)?

CUBES will enable studies of accretion at low metallicities, as well as the effects of local UV fields on accretion and winds – weak fields should not influence the disks, whereas strong fields may modify the ionisation rate in the disk leading to larger mass-loss rates ([39]).

CUBES can be a self-standing instrument for this science case, but YSO crowding may represent an issue for the farthestmost SFRs reachable with the instrument.

5.2 Winds and outflows

As mentioned in Sect. 2.3, the outflow activity in YSOs is a phenomenon strictly related to accretion at different mass regimes. The study of such outflows enables us to elucidate the relationship between mass ejection and accretion, and test the universality of the star formation mechanism as a function of central YSO mass.

In particular, forbidden lines from the UV to the NIR spectral domain can be used to measure the physical properties (density, temperature and ionisation fraction) of the different outflow manifestations using diagnostic tools specifically designed for the purpose. Analysis combining lines at different wavelengths originating from various excitation regimes is important, as applied to CTTS jets observed with X-Shooter ([13], [37]) and more recently with the GIARPS instrument ([38]) at much higher resolution. The CUBES + UVES combination will provide sufficient sensitivity and resolution

to apply such diagnostic tools to studies of fainter and more distant YSOs jets than possible so far.

To this aim, the CUBES spectral range covers several key lines for the study of jets/winds in YSOs. We already mentioned the importance of the [O II] 3726 Å line, in combination with the [O I] 6300 Å line, to estimate the ionization degree of the jets/winds plasma. Other important lines providing complementary information or tracing excitation regimes not probed by optical/IR lines are also present in the CUBES + UVES range. For example, the [S II] doublet at 4069/4076 Å is a useful diagnostic of dense winds in protoplanetary disks ([12] and references therein). Also, the little-studied [Ne III] 3869 Å line signals the presence of high-energy photons, thus probing either high velocity (> 100 km/s) shocks or X-ray heating [52, 53]. The two scenarios can potentially be discriminated through CUBES + UVES velocity-resolved observations.

Finally, the NUV spectral range includes several bright [Fe II] and [Fe III] lines produced from high energy levels, which are therefore good tracers of the temperature of the ionised gas. The observation of [Fe III], combined with [Fe II], allows the simultaneous determination of temperature, density and degree of ionisation, as well as a precise estimate of the Fe abundance in the gas. The relevant non-LTE models required to predict the line fluxes already exist (e.g., [36], [37]).

This analysis approach can be applied to a large sample of sources having different stellar and accretion properties. In addition, the CUBES spectral resolution will enable us to distinguish the different kinematical wind components and separately study the properties of the jets and of the slow winds, as well as investigating whether the relative importance of these two outflow components changes with age, when the contribution of photo-evaporation is expected to be dominant.

Following determination of the physical parameters, the mass ejection rate, \dot{M}_{out} , can be derived from the luminosity of spectrally-resolved forbidden lines. This will allow us to measure the $\dot{M}_{\text{out}}/\dot{M}_{\text{acc}}$ parameter, which critically depends on the jet launching mechanism, and in turn to infer possible variations in the mass loss efficiency due to modifications of the inner disk magnetic and physical properties.

A UVES link would be required for this science case, although not necessarily simultaneous.

6 Summary and conclusions

The CUBES science case on accretion and outflows in YSOs has been presented. The performance of CUBES

in terms **mainly of sensitivity in the NUV (3000–4050 Å) will allow us to broaden** investigations of the evolution of circumstellar disks, by studying the accretion, jets/winds and photo-evaporation processes down to the low-mass, brown dwarf regime **and in more distant YSOs than done so far**. In particular CUBES will enable:

- more precise flux measurements of continuum and emission lines in the NUV. **Contemporaneous photometric observations in the same spectral range will be needed in case the CUBES flux calibration will not be precise at the 15% level or better.**
- **detection** of weak emission lines (and their line morphology), in particular for the Ca II H&K and high-H lines, which are diagnostics of the accretion funnel flows.
- investigation of the physical conditions of the inflowing gas via precise Balmer decrement determinations, including the high-order Balmer lines.
- refinement of the $L_{\text{acc}}-L_{\text{line}}$ relationships by including Balmer lines with a high quantum number.
- better definition of the Balmer jump, as well as detection of weak emission lines, allowing for studies of low-accretion YSOs, including objects in the latest stages of evolution.
- studies of accretion and outflows in very low-mass brown dwarfs, and to study YSOs at much larger distances than done so far, enabling investigation of the effects of metallicity and external UV-radiation on accretion and winds.

In conclusion, CUBES observations of YSOs will lead to a step-change in the study of accretion and outflows in solar-type young stars hence, on protoplanetary disc evolution, as the spectrograph will enable investigation of targets that are several magnitudes fainter than those reachable with current instrumentation.

Acknowledgements We very much thank the two anonymous referees for their comments and suggestions. Financial support from the project PRIN INAF 2019 "Spectroscopically tracing the disk dispersal evolution (STRADE)" is warmly acknowledged. This research made use of the SIMBAD database, operated at the CDS (Strasbourg, France).

References

1. Alcalá, J. M., Natta, A., Manara, C., et al., X-shooter spectroscopy of young stellar objects. IV. Accretion in low-mass stars and substellar objects in Lupus, *Astronomy & Astrophysics*, 561, p. 2 (2014)
2. Alcalá, J. M., Manara, C., Natta, A., et al., X-shooter spectroscopy of young stellar objects in Lupus. Accretion properties of class II and transitional objects, *Astronomy & Astrophysics*, 600, p. 20 (2017)
3. Alcalá, J.M., Manara, C.F., France, K. et al., HST spectra reveal accretion in MY Lupi, *Astronomy & Astrophysics*, 629, p. 108 (2019)
4. Alcalá, J.M., Gangi, M., Biazzo et al., GIARPS High-resolution Observations of T Tauri stars (GHOsT). III. A pilot study of stellar and accretion properties, *Astronomy & Astrophysics*, 652, p. 72 (2021)
5. Alencar, S. H. P., Bouvier, J., Walter, F. M. et al., Accretion dynamics in the classical T Tauri star V2129 Ophiuchi, *Astronomy & Astrophysics*, 541, p. 116 (2012)
6. Andrews, S. M., Wilner, D. J., Espaillat, C., et al., Resolved Images of Large Cavities in Protoplanetary Transition disks, *Astrophysical Journal*, 732, p. 42 (2011)
7. Andrews, S. M., Huang, J., Pérez, L. M. et al., The disk Substructures at High Angular Resolution Project (DSHARP). I. Motivation, Sample, Calibration, and Overview, *Astrophysical Journal letters*, 869, p. 41 (2018)
8. Antonucci, S., Nisini, B., Giannini, T. et al., X-shooter spectroscopy of young stellar objects VI. H I line decrements, *Astronomy & Astrophysics*, 99, p. 105 (2017)
9. Ansdell, M., Williams, J. P., van der Marel, N. et al., ALMA Survey of Lupus Protoplanetary disks. I. Dust and Gas Masses, *Astrophysical Journal*, 228, p. 46 (2016)
10. Ansdell, M., Williams, J. P., Trapman, L. et al., ALMA Survey of Lupus Protoplanetary disks. II. Gas Disk Raii, *Astrophysical Journal*, 473, p. 123 (2018)
11. Aoyama, Y., Marleau, G.-D., Ikoma, M., Mordasini, Ch., Comparison of Planetary H α -emission Models: A New Correlation with Accretion Luminosity, *Astrophysical Journal*, 917, p. 30 (2021)
12. Ballabio, G., Alexander, R. D., Clarke, C. J., Forbidden line diagnostics of photoevaporative disc winds, *M.N.R.A.S.*, 496, p. 2932 (2020)
13. Bacciotti, F., Whelan, E. T. Alcalá, J.M. et al. , The First X-shooter Observations of Jets from Young Stars, *Astrophysical Journal*, 737, p. 26 (2011)
14. Barenfeld, S. A., Carpenter, J. M., Ricci, L. et al., ALMA Observations of Circumstellar Disks in the Upper Scorpius OB Association, *Astrophysical Journal*, 827, p. 142 (2016)
15. Basri, G. & Batalha, C., Hamilton Echelle Spectra of Young Stars. I. Optical Veiling , *Astrophysical Journal*, 363, p. 654 (1990)
16. Biazzo, K., Alcalá, J. M., Covino, et al., The Chamaeleon II low-mass star-forming region: radial velocities, elemental abundances, and accretion properties, *Astronomy & Astrophysics*, 547, p. 104 (2012)
17. Biazzo, K., Beccari, G., De Marchi, G., Panagia, N., Photometric Determination of the Mass Accretion Rates of Pre-main-sequence Stars. VI. The Case of LH 95 in the Large Magellanic Cloud, *Astrophysical Journal*, 875, p. 51 (2019)
18. Bonito, R., Orlando, S., Argiroffi, C. et al., Magnetohydrodynamic Modeling of the Accretion Shocks in Classical T Tauri Stars: The Role of Local Absorption in the X-Ray Emission, *Astrophysical Journal*, 795, L34
19. Calvet, N., Muzerolle, J., Briceño, C. et al., The Mass Accretion Rates of Intermediate-Mass T Tauri Stars, *Astronomical Journal*, 128, p. 129 (2004)
20. Cazzoletti, P., Manara, C. F., Baobab Liu, H. et al., ALMA survey of Class II protoplanetary disks in Corona Australis: a young region with low disk masses, *Astronomy & Astrophysics*, 626, p. 11 (2019)
21. Cieza, L. A., Schreiber, M. R., Romero, G. A. et al., The Nature of Transition Circumstellar disks. I. The Ophiuchus Molecular Cloud, *Astrophysical Journal*, 712, p. 925 (2010)

22. Cody, A. M. & Hillenbrand, L. A., Precision Photometric Monitoring of Very Low Mass σ -Orionis Cluster Members: Variability and Rotation at a Few Myr, *Astrophys. Journal Suppl. Series*, 191, p. 389 (2010)
23. Costigan, G., Scholz, A., Stelzer, B., et al., LAMP: the long-term accretion monitoring programme of T Tauri stars in Chamaeleon I, *M.N.R.A.S.*, 427, p. 1344 (2012)
24. Costigan, G., Vink, J. S., Jorick, S., et al. Temperaments of young stars: rapid mass accretion rate changes in T Tauri and Herbig Ae stars, *M.N.R.A.S.*, 440, p. 3444 (2014)
25. Cusano, F., Ripepi, V., Alcalá, J. M., et al., Pre-main-sequence stars in the star-forming complex Sh 2-284, *M.N.R.A.S.*, 410, p. 227 (2012)
26. De Marchi, Guido; Panagia, N., Beccari, G., Photometric Determination of the Mass Accretion Rates of Pre-main-sequence Stars. V. Recent Star Formation in the 30 Dor Nebula, *Astrophysical Journal*, 846, p. 110 (2017)
27. Donati, J. F., Landstreet, J. D., Magnetic Fields of Non-degenerate Stars, *Annual Review of Astronomy & Astrophysics*, 47, p. 333 (2009)
28. Ercolano, B., Pascucci, I., The dispersal of planet-forming disks: theory confronts observations, *Royal Society Open Science*, Volume 4, Issue 4, id.170114 (2017)
29. Espaillat, C. C., Herczeg, G.J., et al., The ODYSSEUS Survey. I. Motivation and First Results: Accretion, Ejection, and disk Irradiation of CVSO 109, *Astrophysical Journal*, submitted
30. Fang, M., Pascucci, I., Edwards, S. et al., A New Look at T Tauri Star Forbidden Lines: MHD-driven Winds from the Inner disk, *Astrophysical Journal*, 868, p. 28 (2018)
31. Frasca, A., Biazzo, K., Alcalá, J.M. et al., X-shooter spectroscopy of young stellar objects in Lupus: Atmospheric parameters, membership, and activity diagnostics, *Astronomy & Astrophysics*, 602, p. 33 (2017)
32. Frasca, A., Boffin, H.M.J., Manara, C. et al., PENELLOPE II. CVSO 104: a pre-main sequence close binary with an optical companion in Ori OB1, *Astronomy & Astrophysics*, in press
33. Fitzpatrick, E. L., Massa, D., Gordon, K. D. et al., An Analysis of the Shapes of Interstellar Extinction Curves. VII. Milky Way Spectrophotometric Optical-through-ultraviolet Extinction and Its R-dependence, *Astrophysical Journal*, 886, p. 108 (2019)
34. Gangi, M., Nisini, B., Antonucci, S. et al., GIARPS High-resolution Observations of T Tauri stars (GHOT). II. Connecting atomic and molecular winds in protoplanetary disks, *Astronomy & Astrophysics*, 643, p. 32 (2020)
35. Genoni, M., Landoni, M., Cupani, G. et al., The CUBES Instrument model and simulation tools, ExA, in press as part of the CUBES Special Issue
36. Giannini, T., Antonucci, A., Nisini, B., Solving the Excitation and Chemical Abundances in Shocks: The Case of HH 1, *Astrophysical Journal*, 814, p. 52 (2015)
37. Giannini, T., Antonucci, A., Nisini, B. et al., Empirical Determination of Einstein A-coefficient Ratios of Bright [Fe II] Lines, *Astrophysical Journal*, 798, p. 33 (2015a)
38. Giannini, T., Nisini, B., Antonucci, S. et al., GIARPS High-resolution Observations of T Tauri stars (GHOT). I. Jet line emission, *Astronomy & Astrophysics*, 631, p. 44 (2019)
39. Guarcello, M. G., Biazzo, K., Drake, J. J., et al., Dispersal timescale of protoplanetary disks in the low-metallicity young cluster Dolidze 25, *Astronomy & Astrophysics*, 650, p. 157 (2021)
40. Gullbring, E., Hartmann, L., Briceño, C., & Calvet, N., disk Accretion Rates for T Tauri Stars, *Astrophysical Journal*, 492, p. 323 (1998)
41. Gullbring, E., Calvet, N., Muzerolle, J. et al., The Structure and Emission of the Accretion Shock in T Tauri Stars. II. The Ultraviolet-Continuum Emission, *Astrophysical Journal*, 544, p. 927 (2000)
42. Hartigan, P., Kenyon, S. J., Hartmann, L., et al., Optical Excess Emission in T Tauri Stars, *Astrophysical Journal*, 382, p. 617 (1991)
43. Hartigan, P., & Kenyon, S. J., A Spectroscopic Survey of Subarcsecond Binaries in the Taurus-Auriga Dark Cloud with the Hubble Space Telescope, *Astrophysical Journal*, 583, p. 334 (2003)
44. Hartmann, L. in *Accretion Processes in Star Formation*, Cambridge University Press (1998)
45. Hartmann, L., Herczeg, G., Calvet, N., Accretion onto Pre-Main-Sequence Stars, *Annual Review of Astronomy & Astrophysics*, 54, p. 135 (2016)
46. Herczeg, G., & Hillenbrand, L. A., UV Excess Measures of Accretion onto Young Very Low Mass Stars and Brown Dwarfs, *Astrophysical Journal*, 681, p. 594 (2008)
47. Ingleby, L., Calvet, N., Herczeg, G. et al., Accretion Rates for T Tauri Stars Using Nearly Simultaneous Ultraviolet and Optical Spectra, *Astrophysical Journal*, 767, p. 112 (2013)
48. Jayawardhana, R., Coffey, J., Scholz, A., Brandeker, A., & van Kerkwijk, M. H., Accretion disks around Young Stars: Lifetimes, disk Locking, and Variability, *Astrophysical Journal*, 648, p. 1206 (2006)
49. Johns-Krull, C. M., Chen, W., Valenti, J. A. et al., Magnetically Controlled Accretion on the Classical T Tauri Stars GQ Lupi and TW Hydrae, *Astrophysical Journal*, 765, p. 11 (2013)
50. Kunitomo, M., Suzuki, T. K., & Inutsuka, Shuichiro, Dispersal of protoplanetary discs by the combination of magnetically driven and photoevaporative winds, *M.N.R.A.S.*, 492, p. 3849. (2020)
51. Kwan, J., & Fischer, W., Origins of the H, He I and Ca II line emission in classical T Tauri stars, *M.N.R.A.S.*, 411, p. 2383 (2011)
52. Liu, Chun-Fan, Shang, Hsien, Walter, Frederick M., Herczeg, Gregory J., Velocity-resolved [Ne III] from X-Ray Irradiated Sz 102 Microjets, *Astrophysical Journal*, 786, p. 99 (2014)
53. Liu, C.-F., Shang, H., Herczeg, G. J., et al., Revealing Ionization Conditions of Sz 102 with Spatially Resolved [Ne III] Microjets, *Astrophysical Journal*, 909, p. 196 (2021)
54. Long, F., Herczeg, G. J., Harsono, D. et al., Compact disks in a High-resolution ALMA Survey of Dust Structures in the Taurus Molecular Cloud, *Astrophysical Journal*, 882, p. 49 (2019)
55. Lynden-Bell, D., & Pringle, J. E., The evolution of viscous disks and the origin of the nebular variables, *M.N.R.A.S.*, 168, p. 603 (1974)
56. Manara, C. F., Rosotti, G., Testi, L. et al., Evidence for a correlation between mass accretion rates onto young stars and the mass of their protoplanetary disks, *Astronomy & Astrophysics*, 591, L3 (2016)
57. Manara, C. F., Testi, L., Herczeg, G. J., et al., X-shooter study of accretion in Chamaeleon I. II. A steeper increase of accretion with stellar mass for very low-mass stars?, *Astronomy & Astrophysics*, 604, p. 127 (2017)
58. Manara, C. F., Accretion onto young stars: the key to disk evolution, Perspective article for the *Star Formation Newsletter* 300. p. 6 (2017)
59. Manara, C. F., Frasca, A., Venuti, L. et al., PENELLOPE: The ESO data legacy program to complement the Hubble UV Legacy Library of Young Stars (ULLYSES). I. Survey presentation and accretion properties of Orion

- OB1 and σ -Orionis, *Astronomy & Astrophysics*, 650, p.196 (2021)
60. Merín, B., Jørgensen, J. K., Spezzi, L., et al., The Spitzer c2d Survey of Large, Nearby, Interstellar Clouds. XI. Lupus Observed with IRAC and MIPS, *Astrophys. Journal Suppl. Series*, 177, p. 551 (2008)
61. Merín, B., Brown, J. M., Oliveira, I., et al., A Spitzer c2d Legacy Survey to Identify and Characterize disks with Inner Dust Holes, *Astrophysical Journal*, 718, p. 1200 (2010)
62. Mulders, G. D., Pascucci, I., Manara, C. F., et al., Constraints from Dust Mass and Mass Accretion Rate Measurements on Angular Momentum Transport in Protoplanetary disks, *Astrophysical Journal*, 847, p. 31 (2017)
63. Muzerolle, J., Hartmann, L., & Calvet, N., Emission-Line Diagnostics of T Tauri Magnetospheric Accretion. I. Line Profile Observations, *Astronomical Journal*, 116, p. 455 (1998)
64. Nisini, B., Antonucci, S., Alcalá, J. M., Connection between jets, winds and accretion in T Tauri stars. The X-shooter view, *Astronomy & Astrophysics*, 609, p. 89 (2018)
65. Nisini, B., Antonucci, S., Alcalá, J. M., X-Shooter Survey of Jets and Winds in T Tauri Stars, *ASSP*, 55, p. 103 (2019)
66. Owen, J. E., & Clarke, C. J., Two populations of transition disks?, *M.N.R.A.S.*, 426, L96 (2012)
67. Pascucci, I., Testi, L., Herczeg, G. J., et al., A Steeper than Linear disk Mass-Stellar Mass Scaling Relation, *Astrophysical Journal*, 831, p. 125 (2016)
68. Rigliaco, E., Natta, A., Randich, S., et al., X-shooter observations of the accreting brown dwarf J053825.4-024241, *Astronomy & Astrophysics*, 526, p L6 (2011)
69. Rigliaco, E., Natta, A., Testi, L., et al., X-shooter spectroscopy of young stellar objects. I. Mass accretion rates of low-mass T Tauri stars in σ -Orionis, *Astronomy & Astrophysics*, 548, p 56 (2012)
70. Rosotti, G. P., Clarke, C. J., Manara, C. F., & Facchini, S., Constraining protoplanetary disk evolution using accretion rate and disk mass measurements: the usefulness of the dimensionless accretion parameter, *M.N.R.A.S.*, 468, p. 1631 (2017)
71. van der Marel, N., Williams, J. P., Ansdell, M., et al., Title-Paper, *Astrophysical Journal*, 854, p. 177 (2018)
72. Valenti, J. A., Basri, G., & Johns, C. M., New Insights into the Nature of Transition disks from a Complete disk Survey of the Lupus Star-forming Region, *Astrophysical Journal*, 106, p. 2024 (1993)
73. Venuti, L., Bouvier, J., Flaccomio, E., et al., Mapping accretion and its variability in the young open cluster NGC 2264: a study based on u-band photometry, *Astronomy & Astrophysics*, 570, p. 82 (2014)
74. Vorobyov, E. I., & Basu, S., The Bimodality of Accretion in T Tauri Stars and Brown Dwarfs, *Astrophysical Journal*, 703, p. 922 (2009)
75. White, R., & Hillenbrand, L. A., On the Evolutionary Status of Class I Stars and Herbig-Haro Energy Sources in Taurus-Auriga, *Astrophysical Journal*, 616, p. 998 (2004)
76. Zanutta, A., Atkinson, D., Baldini, V. et al. CUBES Phase-A design overview, ExA, in press as part of the CUBES Special Issue